Proceedings of the 9ICEG
9th International Congress on Environmental Geotechnics
25-28 June, 2023 | Chania, Greece

https://doi.org/10.53243/ICEG2023-247

Pore-scale modeling of multiphysics behavior of permafrost

Y. M. Kim[1], A. Abhinav[2], R. Osan[3], B. Motil[4], I. Cozmuta[5], and T. Baser[6]

[1]*Postdoc, University of Illinois at Urbana-Champaign, IL, USA, email: yeongmin@illinois.edu*

[2]*Graduate Research Assistant, University of Illinois at Urbana-Champaign, IL, USA, email: anshua2@illinois.edu*

[3]*CTO, G-Space, Inc., CA, USA, email: remus@g-space.com*

[4]*VP Microgravity, G-Space, Inc., CA, USA, email: brian@g-space.com*

[5]*Founder and CEO, G-Space, Inc., CA, USA, email: ioana@g-space.com*

[6]*Assistant Professor, University of Illinois at Urbana-Champaign, IL, USA, email: tbaser@illinois.edu*

ABSTRACT

This study focuses on quantifying the response of pore-scale transport properties in a multiphase system involving water, ice, gas, and granules subjected to dynamic thermal conditions. Permafrost is a multiphase medium in which solid (grain and ice) and liquid (water and greenhouse gas) coexist, and significant thermal gradients originated by warming result in dynamic subsurface processes. These processes taken in total exert complicated multiphysics behavior that is beyond the predictability of traditional models. Therefore, this research work aims to elaborate on the fluid transport models to replicate the non-isothermal phenomena by including temperature-dependent parameters and interfacial tension-driven flow. A bench-scale experimental setup was developed to simulate the fluid flow through porous media under applied thermal gradients. The setup is monitored during freeze-thaw cycles by a camera with an arrangement of light sources. The images are analyzed using machine learning enhanced computer vision to differentiate phases, detect a freezing and thawing front, and quantify ice/water ratios. Preliminary results from the experiments reveal that the tools used in this study can successfully characterize transport parameters in permafrost. Future experiments combined with mathematical transport models will contribute to the tailoring of the setup that can be used for the prediction of greenhouse gas emissions from thawing permafrost.

Keywords: Multiphysics, thermal gradient, freezing, image analysis

1 INTRODUCTION

Climate change has a profound impact on the whole world and the subsurface temperatures in the permafrost regions are rising at an alarming rate (Figura et al., 2011; Bloomfield et al., 2013; Menberg et al., 2014). The impact of climate change especially severe in the Arctic, which has been confirmed by climate models and observations (Kurylyk et al., 2013; Richter-Menge and Druckenmiller, 2020). There are various causes of the Arctic amplification, but some important ones related to the land include decreased surface albedo and the release of carbon. The melting of ice and snow reduces the surface's reflectivity, leading to increased absorption of solar radiation and warming of the ground (Hall, 2004). Rising ground temperatures cause permafrost to thaw (Richter-Menge and Druckenmiller, 2020), which can result in the release of carbon from the ground by creating pathways for gas migration and destabilizing gas hydrates and soil organic carbon (Hodgkins et al., 2014). Additionally, the carbon stored in permafrost is substantial. The northern regions are estimated to contain approximately 1672 gigatons of carbon, which is nearly double the amount present in the atmosphere. Approximately 1470 gigatons, or 88%, of this carbon is stored in permafrost soils (Tarnocai et al., 2009). If this carbon is released into the atmosphere, it can have devastating consequences for the environment. It is therefore critical to assess the amount and rate of greenhouse gas emission from thawed permafrost for effective adaptation to climate change.

Permafrost is a multiphase medium in which solid (grain and ice) and fluid (water and greenhouse gas) coexists, and significant thermal gradients originated by warming result in dynamic subsurface

processes. These processes exert complicated multiphysics behavior dependent on the history of freezing or thawing (Abhinav and Baser, 2023) and is beyond the predictability of traditional models. Unlike in a saturated medium, water can be non-uniformly distributed in an unsaturated medium, resulting in varying water permeabilities, and non-linear water potential profile. The introduction of gas-liquid interfaces in addition to liquid-solid interfaces would potentially lead to a significant contribution of interfacial forces towards the overall mass transport phenomenon. The discontinuity in physical and thermal properties and the absorption and emission of latent heat entailed by phase transition of water further encumber modeling works (Baser et al., 2022). Lastly, due to the existence of thermal gradient, models should hold a larger number of variables, which could have been assumed constant in isothermal condition, and additional terms describing thermally-induced or -enhanced processes. Thus, to obtain a gas transport model appropriate for the permafrost subsurface based on a better understanding of multiphysical processes, experimental observations under relevant conditions must be accumulated. This study focuses on the development of a bench-scale experimental setup to simulate fluid flow through porous media subjected to thermal gradients. Image processing and machine learning analysis will be performed to quantify spatio-temporal variations of pore-scale features such as liquid, ice, and gas contents, contact angle, and bubble shape and sizes, and mesoscale quantities like water permeability, gas permeability, and mass flux. The pore-scale properties will be used to deduce the surface tension, water potential, and gaseous pressure which acts as driving forces for mass flux. Experiments using this technique will provide us with valuable data to achieve the ultimate goal of this project which is to integrate the empirical interfacial transport properties into the macro-scale models.

2 METHODS

2.1 Granules and liquid

Glass beads were chosen as a representative material for the granules, which are chemically analogous to sand but mostly free of intraparticle pores. The nominal diameter of 3 mm was selected based on practical considerations, time scale, and the relative importance of interfacial flow. The size is considered large enough to allow measurement of contact angles, water, ice, and gas distribution, and temperature or pressure profiles. On the other hand, a smaller system composed of smaller granules would result in a shorter experimental time scale and a larger number of data sets could be gathered. Furthermore, a 40-mm system filled with 3-mm granules results in a Bond number of 3.5, indicating that the chosen length scales are suitable for observing the effects of both gravitational and interfacial forces. Distilled water was used as the liquid. The research work aims to extend this study with different shapes of granules having different material composition. Using different materials and shape will provide a comparison for the effect of shape and contact angle on the freezing behavior of water.

2.2 Sample container

A flat container was constructed with plexiglass to allow optical inspection of the sample as depicted in Figure 1(a). The sample loading area surrounded by 6-mm-thick walls has a volume of 89 mm x 38 mm x 3 mm allowing the 3-mm granules to be arranged in a single layer. The plexiglass is opened from the middle and beads are inserted. Water is carefully added with the help of a syringe to reach a pre-calculated degree of saturation. A parametric study is performed to investigate the effect of variable degree of saturation on the freezing of the sample. The degree of saturation is therefore varied between 0 and 0.75. Through calculation and trials, it is determined that upon freezing a sample with a degree of saturation greater than 0.75, the formation of ice causes expansion which results in excessive air pressure build up inside the sample. A rubber gasket is employed between the two plates of the sample to ensure no water loss during the experiment. A very thin layer of silicon grease is applied on both sides on the gasket to provide additional security towards watertightness. The two plates are then assembled using screws.

2.3 Hardware for freeze and thaw

Hardware for freezing or thawing a sample was selected or designed to develop a one-dimensional thermal gradient in the sample so that a vertical transport can be induced. That not only allows convenience in the observation and numerical analysis, but also could be a good approximation of the vertical migration of gas from the deep permafrost to the surface. The setup for the freeze-thaw experiments using the sample container is shown in Figure 1(b) through (d). Figure 1(c) depicts the plan

view of the whole setup assembled in the freeze-thaw cabinet. The setup consists of an aluminum plate below the thermally insulated control box, directly in contact with the cooling unit and the heating rod. The inner dimensions of the control box are 39.7 cm x 17.8 cm x 10.8 cm and the camera is placed at a distance of 13 cm from the sample. The setup also consists of two light sources and a light diffuser for proper and even illumination of the Biocell. For cooling and heating operations, the HC-3186S Freeze-Thaw (Humboldt Mfg. Co., USA) is employed as a heat sink and source. During the freezing cycle, a flat cooling unit, which circulates the cooling fluid, absorbs heat in the cabinet. The bottom aluminum plate, directly in contact with the cooling unit attains the same temperature under equilibrium conditions. This temperature is then transmitted to the bottom of the Biocell via an aluminum block connecting the Biocell and the aluminum plate as shown in Figure 1(b). Therefore, the cell is frozen from the bottom while the temperature change around the Biocell is buffered by the insulating control box giving rise to a one-dimensional thermal gradient. The insulation is provided by using polystyrene foam to control the boundary conditions and photo-taking conditions, and to protect the camera from direct cold and heat. This setup was obligatory as the numerical simulations indicated the presence of no freezing front if an ambient temperature exists in the periphery of the Biocell, thus necessitating an insulated box with a temperature slightly above the freezing point of water. During the heating operations, a similar mechanism is achieved by electrical heating rods, in contact with the aluminum plate. With minimum and maximum temperature, and hold times assigned via the control panel, freeze/thaw cycles automatically run based on the temperature of a control sample continuously monitored by a thermocouple. The thermocouple is placed inside a container with sand as shown in Figure 1(d). Additionally, desiccants are added inside the control box to eliminate condensation on the plexiglass during the freezing and thawing operations. By preventing fog on the plexiglass sample container, clear images can be taken during the freezing process.

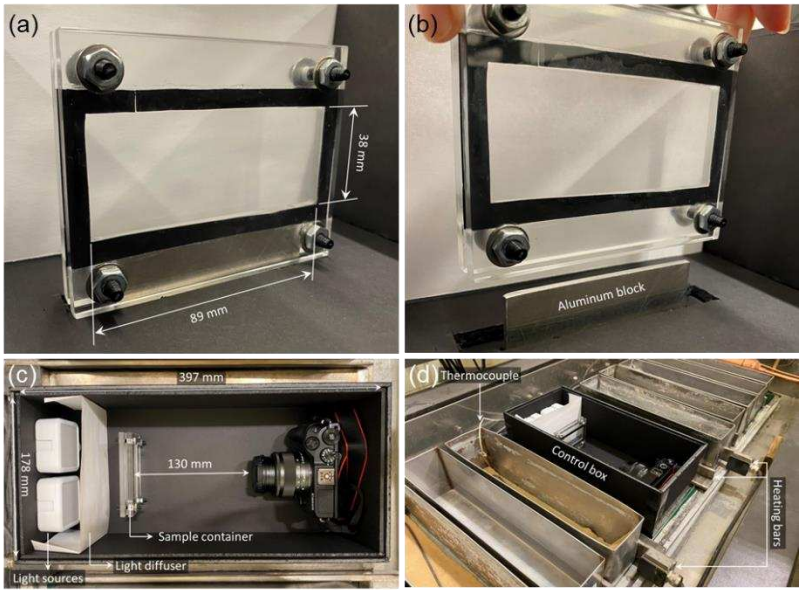

Figure 1. *(a) The sample container; (b) a thermal block inserted to the bottom of the sample container; (c) top view of the control box and elements in it; and (d) the alignment of the control box in the freeze-thaw cabinet.*

2.4 Tuning visual data collection condition

To have a better understanding of the multiphase interactions during the freezing process, images are taken by a camera: Canon EOS M6 Mark II (Canon Inc., Japan). LED lights, Ulanzi VL49 (Shenzhen Ulanzi Technology Co., Ltd., China), were used for better and controlled illumination of the sample. The procedure for collecting images or videos needs to be optimized to clearly capture the interfaces between liquid, ice, gas, and solid, which contain valuable information for quantifying changes in features over space and time. The transparency of glass, water, and air presents a challenge in this regard. To tune the conditions for high-quality images, a set of identical samples was captured under various photo-taking conditions and compared. The intensity and location of lighting, surrounding colors, shutter speed, and ISO were adjusted, while the distance between the object and camera and the aperture setting were kept constant. To measure image clarity, the contrast index was calculated within the sample area using Equation 1.

$$CI = (B_h - B_l) / 255 \quad (1)$$

Where, CI is the contrast index, B_h is the highest brightness and B_l is the lowest brightness.

2.5 Freezing test

A freezing test was conducted to assess the quality of the hardware setup and the optimized data collection conditions in terms of visual data and thermal control. The freeze-thaw cabinet was set to a temperature of -17°C with a freeze hold time of 180 minutes. It took about four hours to reach the desired temperature, which was maintained at approximately -20°C. The empty control box was left in the cabinet for four hours during the freezing phase. Afterwards, a sample composed of glass beads, distilled water, and air was placed in the cabinet and cooled for two hours while a camera captured images every ten seconds in time-lapse video mode under the optimized conditions.

3 RESULTS

3.1 Tuning visual data collection condition

The tuning of some variables such as lighting condition, colour of the background, distance from the camera, shutter speed, aperture, and ISO was performed. The images taken under the tuned condition showed interfaces between phases to be more noticeable. As observed from Figure 2(a), initial images taken without tuning under room light showed glass beads, water, and gas to be barely distinguishable. The value of contrast index was 0.24, which is a very low value. The outlines of clear objects were made more visible by backlighting in a dark surrounding or side lighting on a dark background. The addition of a dark surrounding significantly improved the outcomes, with a CI of 0.58, in which the outlines of glass beads were seen clearly in black which can be observed from Figure 2(b). However, the contrast for the gas-water interfaces was still not large enough. Furthermore, the high resolution of images was

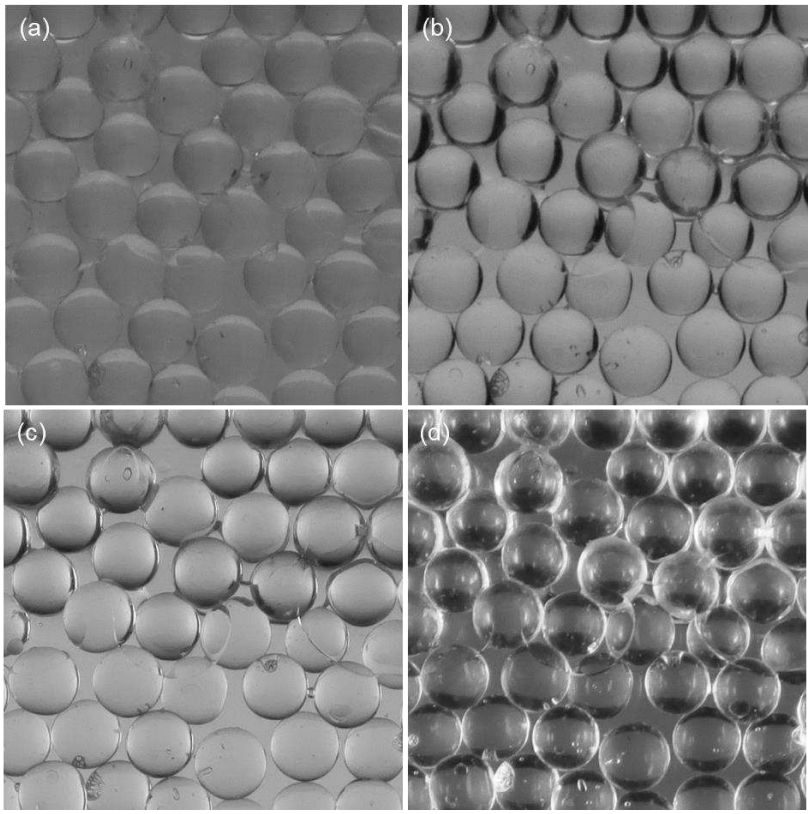

Figure 2. *Selected images of a sample containing glass beads, water, and air: (a) white background and surrounding under room light; (b) white background and dark surrounding under room light; (c) dark surrounding under back light; and (d) dark background under side light.*

hampered by the lack of illumination causing noise. High-resolution images with minimal noise were deemed essential to determine contact angles. By utilizing controlled light sources instead of room light, the contrast was increased up to 0.62 and 0.83 without significant noise under backlighting and side lighting, as observed from Figure 2(c) and 2(d).

Although images with the highest contrast index were produced by side lighting on a dark background, it was preferred to use a bright background as it allowed for further enhancement of the observability through the utilization of dye. The tuned condition was ultimately determined as follows: (1) two lights with 100% intensity behind a white diffuser on the back, (2) black surroundings, (3) the camera at 130 mm, and (4) a shutter speed of 1/800, aperture of 4.5, and ISO of 200.

3.2 Freezing test: quality of visual data

The selection of hardware, sample, and conditions in this work was made with the aim of achieving visual data of high quality that would enable the observation of features at a pore scale. During the freezing test, a video was recorded with a resolution of 3,840 pixels by 2,160 pixels. The region of interest, measuring approximately 2,400 pixels by 1,100 pixels, had a pixel size equivalent to approximately 35 μm in real space. The clarity of the video captured, as depicted in Figure 3(a) through (d), was found to be comparable to the optimal results obtained in Section 3.1 (Figure 2c), and the contrast index (CI) value of 0.64 was also determined to be optimal.

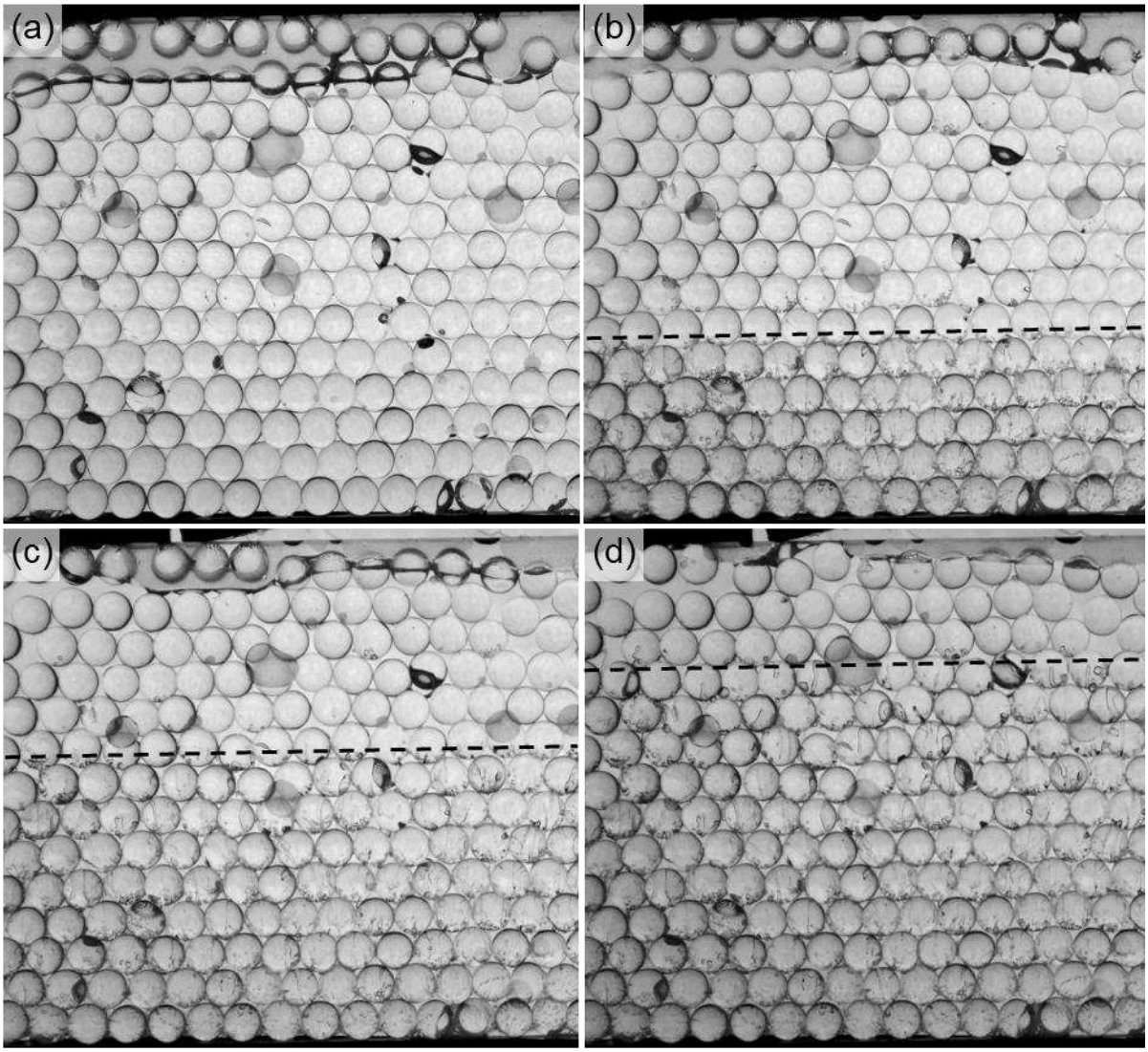

Figure 3. *Screenshots from the video of a sample that was taken during a freezing test, representing (a) 0.5-; (b) 1.0-; (c) 1.5-; and (d) 2.0-hour frozen sample. Dash lines indicate the freezing fronts moving upward.*

3.3 Freezing test: trends in ice development

The screenshots of the video, shown in Figure 3(a) through 3(d), depicts the advancement of a horizontally flat freezing front starting from the point of contact between the 6-mm-thick plexiglass sandwich sample and the conductive block. It can be observed from Figure 3(a) that the air phase, water phase and the solid phase can be easily distinguished visually. Also, the freezing did not start until 30 minutes after the sample was placed inside the control box. Figure 3(b) depicts the visual state of the sample 1 hour after the placement of the sample. It can be observed that the freezing front horizontally advanced from the bottom to the top. Figures 3(c) and (d) show the subsequent movement of the freezing front after 1.5 and 2 hours respectively. The presence of micro-scale bubbles with sizes less than 300 μm and channels, created by the release of air dissolved in water, makes the frozen water visually distinguishable from unfrozen water. The form and movement of the freezing front indicate the existence of a one-dimensional thermal gradient in the vertical direction and highlight the lower boundary as the dominant heat sink, as intended.

The height of the freezing front was estimated from the video that was recorded during the freezing process and was plotted against time as shown in Figure 4. It was observed that the freezing process started after approximately 30 minutes and had reached a height of 29 mm after two hours. The progression of the freezing front appeared to be consistent, with an average velocity of 0.30 mm/min once it had started. If the velocity is maintained, it is estimated that the entire sample can be frozen in a total of 2.6 hours.

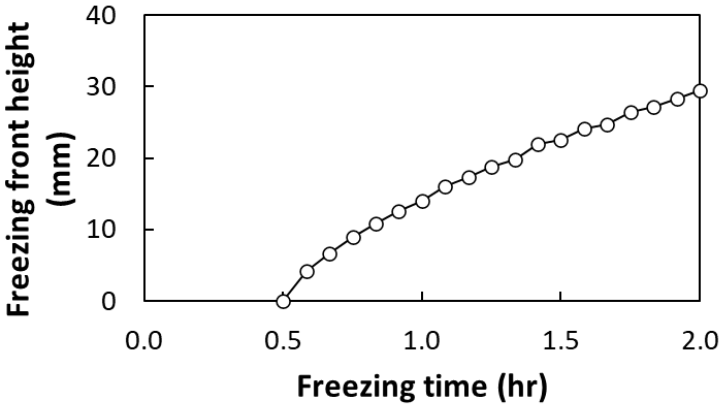

Figure 4. *The advancement of the freezing front during a freezing test.*

4 CONCLUSIONS

This study focused on the development of an experimental setup was proposed to facilitate the observation of multiphysics processes in frozen soils at pore-scale. The setup included a sample container consisting of transparent windows and the ability to hold 3-mm granules in a single layer. Using a high-resolution camera and carefully tuned conditions, visual data was produced that enabled the observation of pore-scale objects and phenomena. In a freezing test conducted with the use of a conventional freeze-thaw cabinet and a thermal control box, a one-dimensional thermal gradient was induced in a sample made up of glass beads, water, and air. The results of the study indicated that the proposed tools could produce partially frozen, unsaturated porous media as a representative of permafrost, allowing for the characterization of transport parameters in permafrost. Future experiments combined with mathematical transport models are expected to further refine the setup, leading to the improved prediction of greenhouse gas emissions from thawing permafrost.

5 ACKNOWLEDGEMENTS

This research was supported by Basic Science Research Program through the National Research Foundation of Korea (NRF) funded by the Ministry of Education (2021R1A6A3A14043794).

REFERENCES

Abhinav, A., & Baser, T. (2023). An Experimental Investigation of Thermally Induced Hydraulic Hysteresis in Frozen Unsaturated Silts. In *Geo-Congress 2023* (pp. 561-571).

Baser, T., Abhinav, A., & Mineyev, I. (2022, December). Determination of Ice Content using Latent Heat during Soil Freezing and Thawing. In *AGU Fall Meeting Abstracts* (Vol. 2022, pp. GC55F-0297).

Bloomfield, J. P., Jackson, C. R., & Stuart, M. E. (2013). Changes in groundwater levels, temperature and quality in the UK over the 20th century: an assessment of evidence of impacts from climate change

Figura, S., Livingstone, D. M., Hoehn, E., & Kipfer, R. (2011). Regime shift in groundwater temperature triggered by the Arctic Oscillation. *Geophysical Research Letters*, *38*(23).

Hall, A. (2004). The role of surface albedo feedback in climate. Journal of climate, 17(7), 1550-1568.

Hodgkins, S. B., Tfaily, M. M., McCalley, C. K., Logan, T. A., Crill, P. M., Saleska, S. R., ... & Chanton, J. P. (2014). Changes in peat chemistry associated with permafrost thaw increase greenhouse gas production. Proceedings of the National Academy of Sciences, 111(16), 5819-5824.

Kurylyk, B. L., Bourque, C. A., & MacQuarrie, K. T. (2013). Potential surface temperature and shallow groundwater temperature response to climate change: an example from a small forested catchment in east-central New Brunswick (Canada). *Hydrology and Earth System Sciences*, *17*(7), 2701-2716.

Menberg, K., Blum, P., Kurylyk, B. L., & Bayer, P. (2014). Observed groundwater temperature response to recent climate change. *Hydrology and Earth System Sciences*, *18*(11), 4453-4466.

Richter-Menge, J., & Druckenmiller, M. (2020). State of the climate in 2019. Arctic, 101(8), S239-S286.

Tarnocai, C., Canadell, J. G., Schuur, E. A., Kuhry, P., Mazhitova, G., & Zimov, S. (2009). Soil organic carbon pools in the northern circumpolar permafrost region. Global biogeochemical cycles, 23(2).